

Approaches for Fuel Cell Stack Modeling and Simulation with COMSOL Multiphysics®

C. Siegel^{*1,2}, G. Bandlamudi^{1,2}, P. Beckhaus¹ and A. Heinzl^{1,2}

¹Zentrum für BrennstoffzellenTechnik (ZBT) GmbH, Duisburg, Germany

²University of Duisburg-Essen, Institut für Energie- und Umweltverfahrenstechnik, Duisburg, Germany

*Corresponding author: Zentrum für BrennstoffzellenTechnik (ZBT) GmbH, Carl-Benz-Straße 201, D-47057 Duisburg, Germany, c.siegel@zbt-duisburg.de

Abstract: This study highlights the possibility of using COMSOL Multiphysics® for solving large scale fuel cell stack models. First, the fluid flow behaviour and pressure distribution of fuel cell stacks with different number of cells is simulated, taking the full 3D Navier-Stokes equations into account. It is seen that the amount of fluid is not equally distributed throughout the cells within a stack. Second, a theoretical study of a complete 3D two cell high temperature PEM (HTPEM) stack is presented. This model geometry consists of all parts ranging from the aluminium endplates to the high temperature stable membrane-electrode-assembly (MEA). All governing equations are solved within the respective subdomains for typical operating conditions. Computational aspects are discussed regarding v3.5a and v4.0a of the software.

Keywords: Polymer-electrolyte-membrane fuel cell (PEMFC), HTPEM, fuel cell stack model, fluid flow, large scale modeling, CFD

1. Introduction

Fuel cell systems are gaining increased attention as alternative power generation source for diverse hydrogen applications. Simplification and optimization of such a complex system not only includes peripheral components (e.g. pumps, valves) but also the fuel cell stack in terms of alternative designs. Solving complete single fuel cell models is nowadays possible with COMSOL Multiphysics® running on massive computer hardware. Nevertheless, the larger the MEA area becomes the larger the memory requirements are. Same is the case for higher number of cells in a fuel cell stack.

Several computationally undemanding stack modeling techniques (i.e. hydraulic network approach, analytical and/or empirical calculations, dynamic system modeling for control applications) are generally adopted for

predicting the overall performance of a complete stack [1-3]. Beside all benefits of efficient and fast calculations, detailed information concerning spatial quantities distribution can hardly be achieved with the above mentioned methods. In the last years the numbers of published works on computational fluid dynamics (CFD) fuel cell stack modeling increased. In 2006 Liu et al. [4] came up with a numerical simulation of a mini six cell PEM stack and compared the simulation results to experimental tests. The model could only be solved on personal computers using reasonable simplifications. The flow distribution in the manifold of a 72 cell PEM stack was modeled in 2D in [5], accounting for pressure loss and fluid flow distribution. Shimpalee et al. [6] combined experiments and numerical simulations to analyze the behaviour of a portable six cell PEM short stack. A CFD based methodology was used to predict quantities behaviour. Recently, interesting results on combined particle image velocimetry (PIV) and CFD analysis of fuel cell manifolds were published in [7]. Results showed that the inlet piping geometry can have a significant influence of the fluid flow distribution throughout the stack.

Complete 3D fuel cell stack modeling and simulation is able to deliver detailed theoretical inside information that may include:

- Fluid flow within the manifold of stacks (possibly turbulent at high flow rates)
- Locating fluid expansion (e.g. sudden expansion) and contraction zones
- Evaluation of possible recirculation zone (accumulation of water)
- Overall pressure loss and fluid flow distributions throughout the stack
- Prediction of the cell to cell fluid flow distribution within a stack

- Related cell to cell operational behaviour for given operating conditions

The objective of this work is to highlight possible approaches when using COMSOL Multiphysics® as a tool for solving large scale fuel cell stack models. This work is divided in two parts and reports:

1. the fluid flow behaviour within fuel cell stacks with different numbers of cells (from single cell to 15 cells) using simplified gas piping geometries
2. a theoretical study of a complete 3D two cell HTPEM stack as a practical example

Beside, emphasis is put on computational aspects and hardware requirements when solving these problems with different versions of the software (namely v3.5a – 3.5.0.608 and v4.0a – 4.0.0.993).

2. Model Geometries

2.1 Gas Piping

The complete gas piping geometry of a stack is generated by repeating the single cell flow field geometry that was modeled and simulated in earlier works [8]. Additionally, the inlet and outlet manifolds geometries (i.e. inlet and outlet header) are represented in a simplified way. It must be noted that only the fluid flow at the cathode side is investigated (with gas properties corresponding to air). Fluid flow at the anode side is assumed to be smooth and equally distributed. Fig.1 shows the 10 cell stack gas piping geometry (exemplary).

2.2 Two Cell HTPEM Stack

The geometry of the two cell HTPEM stack consists of two aluminum endplates, four heating elements, two gold plated copper current collectors, two insulation sheets, four bipolar plates (including the drilled six channel parallel serpentine flow field), and two MEA consisting of two gas diffusion layers and the membrane (Fig.2).

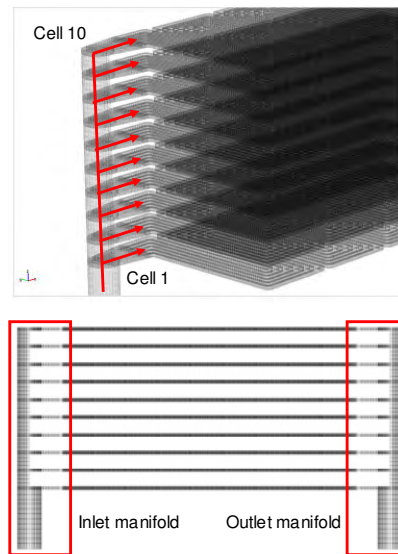


Figure 1. 10 cell gas piping geometry (gas manifolds and gas flow channels → six channel parallel serpentine flow field).

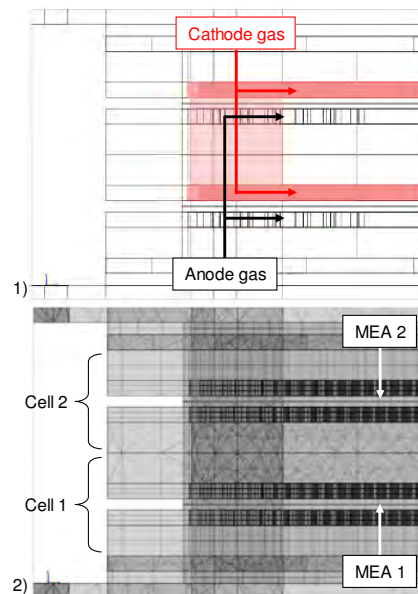


Figure 2. Zoom box of the two cell HTPEM stack geometry. 1) Geometry in y-z-plane with anode/cathode gas manifold and gas flow channels (highlighted in black/red). 2) Mixed free/mapped mesh including cell 1 (MEA 1) and cell 2 (MEA 2).

3. Subdomain and Boundary Equations

3.1 Gas Piping

The same transport equations as in [8] were used to study the fluid flow behaviour. Laminar fluid flow (incompressible Navier-Stokes application mode) is assumed within the gas manifolds and the flow field. At the inlet, the total mass flow rate ($[\text{l}\cdot\text{min}^{-1}]$) was defined. At the outlet a pressure ([Pa]) condition was applied. A continuity or no-slip condition was defined at all remaining boundaries. Some of the above made assumptions may not be valid for a higher number of cells in a stack (higher gas flow rates) as the flow within the in-, and outlet manifold may become laminar/transitional as stated in [7].

Two different gas flow rates (or operating conditions) were defined according to 20 [A], 40 [A], and 60 [A] load current:

- Dry operating conditions: air as cathode gas at 21°C , $St_C = 2.5$ [-], $p = 1.01325 \cdot 10^5$ [Pa]
- Wet operating conditions: air saturated at 60°C as cathode gas, $St_C = 2.5$ [-], $p = 1.01325 \cdot 10^5$ [Pa]

3.2 Two Cell HTPEM Stack

For the two cell stack model, very similar transport equations (momentum/mass, species, charge, energy) were used herein, as proposed in [9]. Anyways, this set up slightly differs from the previous ones:

- Fluid-phase temperature equals solid-phase temperature (gases are supposed to be heated up to 160°C before entering the cell)
- A constant solid-phase temperature is defined at the boundaries of the heating elements according to experimental tests ($T_s = 190^\circ\text{C}$)
- A mass flux boundary condition (reaction rates) is used at both electrodes since they are treated as infinitesimal thin layers
- A heat flux boundary condition is applied at most outer boundaries (aluminum endplates, gold plated copper current collectors, and bipolar plates). Ambient temperature $T_{\text{amb.}} = 21^\circ\text{C}$.

The following operating conditions were carefully defined: 1.2 [V] cell voltage, hydrogen and dry air as anode and cathode gas, $St_A = 1.3$ [-], $St_C = 2.5$ [-], $p = 1.01325 \cdot 10^5$ [Pa], $T_f = 160^\circ\text{C}$.

4. Geometry Meshing and Solving Large Scale Models

4.1 Gas Piping

When solving large scale fuel cell stack models with COMSOL Multiphysics®, one should carefully mesh the geometry in order to reduce the number of degrees of freedom (DOF) without affecting the simulation results (mesh independency tests must be performed). The gas piping geometries were solved using a (parametric) direct solver (PARDISO) and/or an iterative solver (BiCGStab / MG) in order to compare computational aspects. In most cases, best results were achieved by ramping up parameters to the desired values, respectively by a series of dummy simulations.

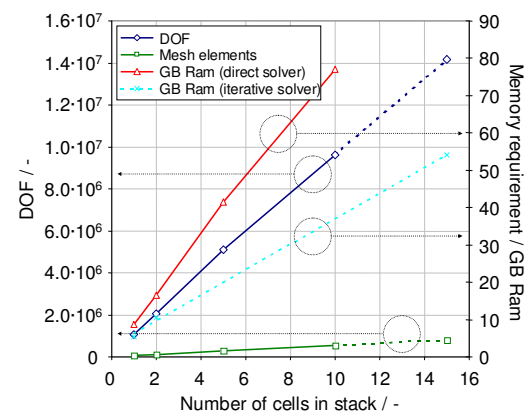


Figure 3. Recorded details while solving the different gas piping geometries (values recorded for v3.5a of the software).

Fig.3 depicts recorded details concerning meshing and solving of the gas piping geometries. The final mesh consisted of prism elements only and ranged from 60,012 (1 cell) to 800,172 (15 cells) with an overall minimum element quality of 0.0429. The memory requirements for the direct solver ranged from 8.7 GB Ram to 77 GB Ram when using v3.5a of the software. The 15 cell gas piping geometry

could only be solved using an iterative solver (total memory allocation 54 GB Ram).

Having the values in Fig.3 one can easily guess the total number of elements, the number of DOF, and the memory requirements to model an n cell gas piping geometry. For these particular fluid flow problems, the iterative solver only required less than half the memory of the direct solver. A very similar behaviour was recorded for v3.5a and v4.0a of the software.

The computational clock times when using v3.5a of the software were recorded to be 754-1,306 s (one cell), 1,328-12,090 s (two cells), and $\pm 20,275$ s (five cells) depending on the operating conditions. With v4.0a of the software, the computational clock time for a one cell gas piping geometry was 751 s (MUMPS), respectively 789 s (PARDISO). With iterative solvers the same problem was solved in 2,538 s (GMRES / MG) respectively 2,697 s (BiCGStab / MG) for 20 [A] load and dry operating conditions. The two cell gas piping geometry was solved within 1,515s (MUMPS) respectively 1,515 s (PARDISO), again for 20 [A] load and dry operating conditions. It must be noted that these values strongly depend on the computer hardware and the solver configuration (e.g. parameter values). The computational time for the 10 and 15 cell stack could not be recorded because several dummy simulations had to be performed until a converged solution was returned.

4.2 Two Cell HTPeM Stack

As for the two cell HTPeM stack example, different solver settings were used to solve the problem. Momentum/mass transport was solved with a direct solver (PARDISO). According to our tests, it was not possible to achieve a converged solution with an iterative solver when simulating a coupled Navier-Stokes to Brinkman (coupling of free flow to porous media flow) problem in 3D with v3.5a (contrary to v4.0a). Species, charge, and energy transport was solved with an iterative solver (GMRES / 3 level MG / SOR(U) as pre-, and postsmoother / PARDISO as coarse solver). The total number of DOF for this model was 20,434,078, resulting from 1,520,453 finite elements (834,209/686,244 tetrahedral/prism). The total computational clock

time at a cell voltage of 1.2 [V] was $\pm 80,000$ s (shorter/longer calculation times for lower/higher current densities observed). Fig.4 shows the recorded details while solving the model (memory requirements up to 68 GB Ram when solving e.g. the mass/species/charge application modes).

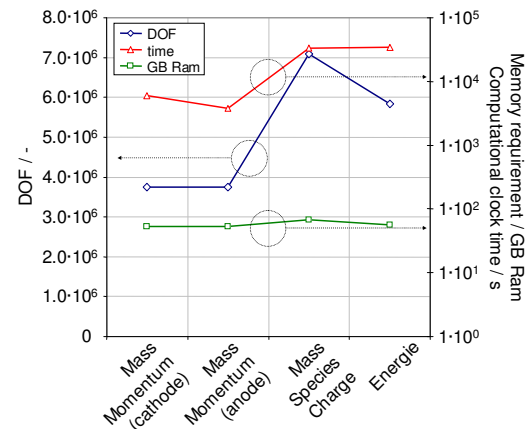


Figure 4. Recorded details while solving the complete two cell HTPeM stack model (values recorded for v3.5a of the software).

5. Results and Discussion

5.1 Gas Piping

The channel to land ratio of the flow field is constant for all geometries (1 [mm] / 1 [mm]), channel depth 1 [mm]). From the results, it can be seen that possible recirculation zone(s) exist at the outlet of the flow field, respectively inlet of the manifold (Fig.5). In these regions, liquid water may accumulate quickly. Additionally, the presents of recirculation zones leads immediately to higher pressure losses.

The mean channel velocity was calculated by using subdomain integration. For all gas piping geometries the values were between 2.248 [m·s⁻¹] (flow according to 20 [A] load current and dry operating conditions) and 10.15 [m·s⁻¹] (total flow according to 60 [A] load current and wet operating conditions).

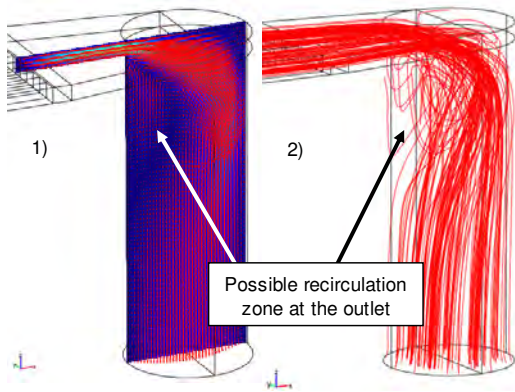


Figure 5. Possible recirculation zone close to the inlet of the gas piping respectively outlet of the six channel parallel serpentine flow field. 1) Velocity vectors and velocity slice plot. 2) Streamline plot of the velocity.

Table 1 lists the mean velocity values within the manifold for different gas piping geometries and different load currents. It is seen that much higher values are present when humidified gases are used. Moreover, it is seen that the mean manifold velocity values are in the range of the mean channel velocity values only for a higher number of cells within a stack.

Table 1: Selected mean velocity values within the manifold (d = dry operating conditions, w = wet operating conditions)

$U_{m,mean}$ [m·s ⁻¹]	20 [A]	40 [A]	60 [A]
1 Cell	0.508 d 0.767 w	1.027 d 1.5512 w	1.547 d 2.337 w
2 Cells	0.8606 d 1.298 w	1.724 d 2.602 w	2.592 d 3.913 w
5 Cells	1.615 d 2.443 w	3.244 d 4.906 w	
10 Cells	2.382 d		

Table 2 lists the pressure losses over selected gas piping geometries for different operating conditions. Similar to the mean velocity values, the pressure losses are higher for wet operating conditions. These values only slightly increase for a higher number of cells, possibly due to the fact that the fluid flow behaviour is calculated laminar herein.

Table 2: Pressure losses over selected gas piping geometries (d = dry operating conditions, w = wet operating conditions)

ΔP [mbar]	20 [A]	40 [A]	60 [A]
1 Cell	6.67 d 11.9 w	17.1 d 30.36 w	30.92 d 55.13 w
2 Cells	6.789 d 11.94 w	17.17 d 30.48 w	31.07 d 55.38 w
5 Cells	6.92 d 12.18 w		

When analyzing the cell to cell fluid flow, no notable difference was observed for a two cell gas piping geometry. Nevertheless, severe differences exist for stacks with a higher number of cells. This maldistribution is comparable to the results presented in [7] and highlighted in Fig.6. The mean velocity is not equally distributed throughout the cells for different stack configurations.

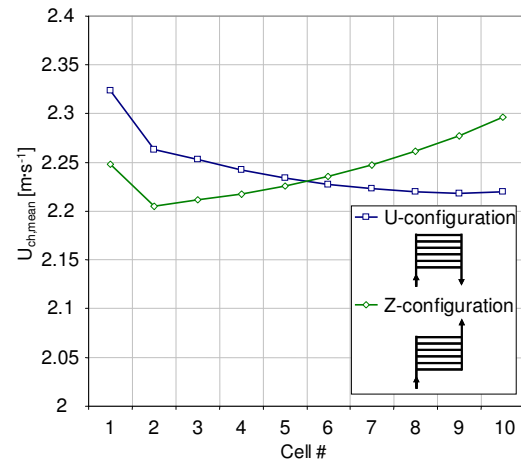


Figure 6. Mean gas channel velocity for different stack configurations (gas flow rates according to 20 [A] load current at given St_c) within a 10 cell gas piping geometry.

For a stack in U-configuration, the highest mean gas channel velocity is seen in the first cells. The mean velocity value within cell number 10 is only 95.5% of the value seen in cell number 1. For a stack in Z-configuration, higher mean gas channel velocities are observed in the cells with the numbers 6-10. A notable difference is seen between the first and the second cell within the

stack for both configurations. In fact, this difference again increases with a higher number of cells in a stack. Thus, it is expected that for a stack consisting up to 70-100 cells, the first ten cells may receive considerably less gas when using an unfavorable manifold configuration.

5.2 Two Cell HTPEM Stack

Due to space limitation, only two selected quantities distributions are discussed in this work i.e. the potential and temperature distribution. Fig.7 depicts the solid-, and membrane-phase potential at different positions along the z-axis. At the anode side gold plated copper current collector, the cell voltage is zero. It is shown how the two individual cells contribute to the total cell voltage of 1.2 [V] (fixed at the cathode side gold plated copper current collector).

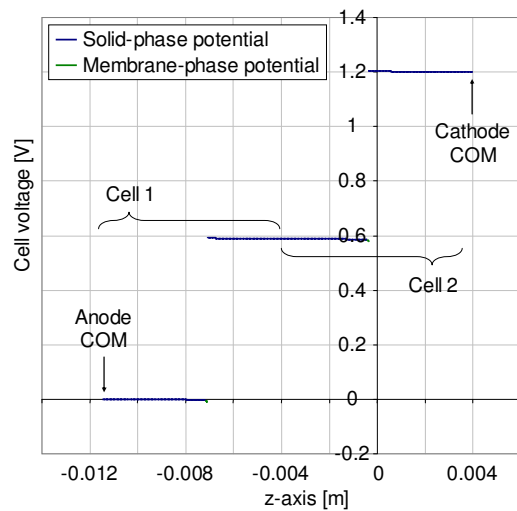


Figure 7. Solid-, and membrane-phase potential along the z-axis ($x/x_{\max} = 0.1$, $y/y_{\max} = 1/2$) through the two cell HTPEM stack.

The resulting mean overpotential (for the electrochemical reactions) at the cathode and anode side reaction layers is calculated using boundary integration. The following values are returned: Cell 1 → anode 0.00384 [V]; Cell 1 → cathode -0.482858 [V]; Cell 2 → anode 0.003859 [V]; Cell 2 → cathode -0.496745 [V]. From the simulations it is seen that the fluid flow through both cells is almost equal. Consequently, the current density within both cells is calculated

to be 4,239.25 [$\text{A}\cdot\text{m}^{-2}$] (Cell 1) vs. 4,237.97 [$\text{A}\cdot\text{m}^{-2}$] (Cell 2).

For a higher number of cells in a stack, the flow will be much more unevenly distributed (as shown in Fig.6), significantly affecting the current density distribution within the individual cells.

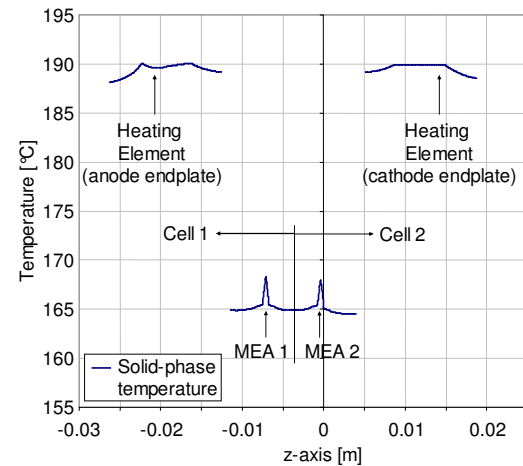


Figure 8. Solid-phase temperature along the z-axis ($x/x_{\max} = 0.1$, $y/y_{\max} = 1/2$) through the two cell HTPEM stack.

Another quantity that should be highlighted is the solid-phase temperature. Fig.8 represents the temperature within the different components of the stack. It is seen that the highest temperature is located close to the heating elements. A large temperature gradient is observed over the electric insulation sheet ($\Delta T_s \pm 25^\circ\text{C}$). When operating a four or six cell stack, it is expected that this temperature difference will be reduced since much more heat is produced internally (the stack will be able to sustain the desired operating temperature level by itself).

The temperature over the four bipolar plates is quite uniform with two peaks coming from the heat production within the MEA (mainly within both cathode side reaction layers). Overall, the temperature within the middle of the x-y-plane (center of the stack) is $\pm 5^\circ\text{C}$ higher than the mean operating temperature of 160°C . Along with Fig.9 it is seen that the boundary temperature is lowest (close to 135°C) at the gold plated copper current collectors and bipolar plate boundaries due to the large temperature

difference (heat loss towards the surroundings). This fact should be taken into account when locating the optimal positioning of the set-temperature thermoelement(s) for a stack being operated in a teststand. Results also reveal that a good thermal insulation is crucial when operating small stacks in order to keep the temperature distribution somehow uniform and minimize heating power.

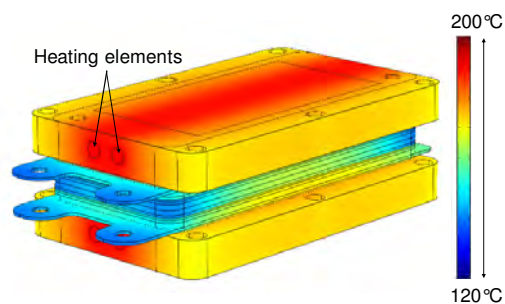


Figure 9. Solid-phase temperature (boundary plot) for defined operating conditions.

7. Conclusions

Laminar fluid flow behaviour within the gas flow channels is widely accepted but should carefully be treated when modeling gas piping geometries. For large stacks the velocity within the manifolds may easily reach up to 60-80 [m·s⁻¹]. A laminar fluid flow application mode might be an oversimplification and pressure losses underestimated since results show that recirculation zones exist and that the cell to cell fluid flow varies. The two cell HTPEM stack example shows that COMSOL Multiphysics® can potentially be used for modeling small fuel cell stacks with adequate computer hardware. For this particular type of problems, a similar performance was observed when it comes to computational clock time and memory requirements for v3.5a and v4.0a of the software. Furthermore, v4.0a shows better convergence behaviour for free flow/porous media flow coupled problems.

8. References

1. Koh, J.-H., Seo, H.-K., Lee, C.G., Yoo, Y.-S., Lim, H.C., Pressure and Flow Distribution in Internal Gas Manifolds of a Fuel-Cell Stack, *J. Power Sources* **115**, 54-65 (2003)

2. Karimi, G., Baschuk, J.J., Li, X., Performance Analysis and Optimization of PEM Fuel Cell Stacks using Flow Network Approach, *J. Power Sources* **147**, 162-177 (2005)
3. Kulikovskiy, A.A., Efficient Parallel Algorithm for Fuel Cell Stack Simulation, *SIAM J. Appl. Math.* **70**, 531-542 (2009)
4. Liu, Z., Mao, Z., Wang, C., Zhuge, W., Zhang, Y., Numerical Simulation of a Mini PEMFC Stack, *J. Power Sources* **160**, 1111-1121 (2006)
5. Chen, C.-H., Jung, S.-P., Yen, S.-C., Flow Distribution in the Manifold of PEM Fuel Cell Stack, *J. Power Sources* **173**, 249-263 (2007)
6. Shimpalee, S., Ohashi, M., Van Zee J.W., Ziegler, C., Stoeckmann, C., Sadeler, C., Hebling, C., Experimental and Numerical Studies of Portable PEMFC Stack, *Electrochim. Acta*, **54**, 2899-2911 (2009)
7. Lebak, J., Andreasen, M.B., Andresen, H.A., Bang, M., Kær, S.K., Particle Image Velocimetry and Computational Fluid Dynamics Analysis of Fuel Cell Manifold, *ASME J. Fuel Cell Sci. Technol.* **7**, 031001-1-031001-10 (2010)
8. Siegel, C., Bandlamudi, G., van der Schoot, N., Heinzl, A., *Large Scale 3D Flow Distribution Analysis in HTPEM Fuel Cells*, Oral presentation, Published in: Proceedings of the European COMSOL Conference, Milan, Italy (2009)
9. Siegel, C., Bandlamudi, G., Heinzl, A., *Modeling Polybenzimidazole/Phosphoric acid Membrane Behaviour in a HTPEM Fuel Cell*, Oral presentation, Published in: Proceedings of the European COMSOL Conference, Hannover, Germany (2008)

9. Acknowledgements



This work was supported by the National Research Fund, Luxembourg (Grant No.: AFR07/007) and by the European Funds for Regional Development and the Region of North Rhine-Westphalia, Germany.